LA-UR-12-24539

Precise determination of the structure factor and contact in a unitary Fermi gas

Sascha Hoinka,[1] Marcus Lingham,[1] Kristian Fenech,[1] Hui Hu,[1]
Chris J. Vale,[1] Joaquín E. Drut,[2,3] and Stefano Gandolfi[3]

[1] *Centre for Atom Optics and Ultrafast Spectroscopy, Swinburne University of Technology, Melbourne 3122, Australia*
[2] *Department of Physics and Astronomy, University of North Carolina, Chapel Hill, NC 27599-3255, USA*
[3] *Theoretical Division, Los Alamos National Laboratory, Los Alamos, New Mexico 87545, USA*

(Dated: September 19, 2012)

We present a high-precision determination of the universal contact parameter in strongly interacting Fermi gases. The contact governs the high-momentum properties (i.e. the short-range correlations) of these systems. The experimental measurement utilises Bragg spectroscopy to obtain the dynamic and static structure factors of ultracold Fermi gases at high momentum in the unitarity and molecular Bose-Einstein condensate (BEC) regimes. We have also performed quantum Monte Carlo calculations of the static properties, extending from the weakly coupled Bardeen-Cooper-Schrieffer (BCS) regime to the strongly coupled BEC case, which show excellent agreement with experiment at the level of a few percent. At unitarity our low temperature measurement provides a new benchmark for the zero temperature homogeneous contact which we find to be 3.33 ± 0.07.

PACS numbers: 67.85.–d, 03.75.Hh, 03.75.Ss, 05.30.Fk

Ultracold atomic gases are unparalleled as a means to quantitatively probe strongly coupled systems which lie at the intersection of condensed-matter [1], nuclear [2, 3] and high-energy physics [4, 5]. In this context, two-component mixtures of fermionic atoms have particular significance as they are generally stable against inelastic decay. These *universal* quantum systems [6–8] are characterized by strong coupling in the form of s-wave interactions of short range r_0 and large scattering length a, such that the only scales left are thermodynamical: the density n or chemical potential μ and the temperature T, just as in a non-interacting gas. This situation, in particular the unitary limit $0 \leftarrow k_F r_0 \ll 1 \ll k_F a \to \infty$, where k_F is the Fermi wavevector [9], represents a major theoretical challenge as there are no small parameters. While there is no exact description, a variety of approximate techniques have been developed; however, these often predict quite different outcomes.

One of the key quantities characterizing these systems is the universal contact parameter C, introduced by Tan [10, 11]. The contact derives from the short-range properties of strongly interacting quantum gases and is the cornerstone of a number of exact relations describing the static and dynamic properties such as the equation of state and dynamic response functions [12–15]. Evaluating these exact relations requires precise knowledge of C itself, which is very challenging to compute with different calculations varying by as much as 10% [16, 17].

In this letter we provide a new benchmark measurement, accurate to the level of 2%, for the contact at unitarity. This measurement is furnished by a precise determination of the dynamic and static structure factors using Bragg spectroscopy. In addition, we present new Quantum Monte Carlo (QMC) calculations accurate to the level of a few percent. Our results indicate that theory and experiment are reaching a new level of convergence, showing that this difficult problem is becoming tractable.

Experimental setup. The experiments presented here use a gas of ^{6}Li prepared in an equal mixture of the $|F = 1/2, m_F = \pm 1/2\rangle$ spin states, evaporatively cooled in a single-beam optical dipole trap. Interactions are tuned to the unitary limit by setting the magnetic field to 833.0 G, close to the pole of the Feshbach resonance. Following evaporation, the cloud of approximately $N/2 = 2.2 \times 10^5$ atoms per spin state is at a temperature of $\sim 0.07 T_F$ where T_F is the local Fermi temperature in the centre of the trap. The atoms are then loaded into a second optical dipole trap produced by a 10 W single frequency 1064nm fibre laser that is spatially filtered before entering the cell to produce a deep trap with large harmonic region. The trapping frequencies in the radial and axial directions are $\omega_x = \omega_y = 2\pi \times 97$ Hz and $\omega_z = 2\pi \times 24.5$ Hz, respectively.

Bragg scattering is performed as in previous work [18, 19]. Two laser beams, detuned by approximately 600 MHz from the nearest atomic transition, illuminate the atom cloud, intersecting at an angle of $2\theta = 84°$. This sets the probe wavevector $k = (4\pi/\lambda)\sin\theta$ where $\lambda = 671$nm. The beams are obtained from the same laser with two different acousto-optic modulators, driven by an amplified signal from a multichannel direct digital synthesizer. This allows us to precisely tune the frequency difference between the two beams ω with a stability better than 1 Hz.

To obtain the dynamic response function we measure the momentum imparted to the cloud for a range of Bragg frequencies. By imaging atoms in both spin states with a short (850 μs) time delay between images we can determine the centre of mass cloud displacement ΔX, which is proportional to the imparted momentum [18], without

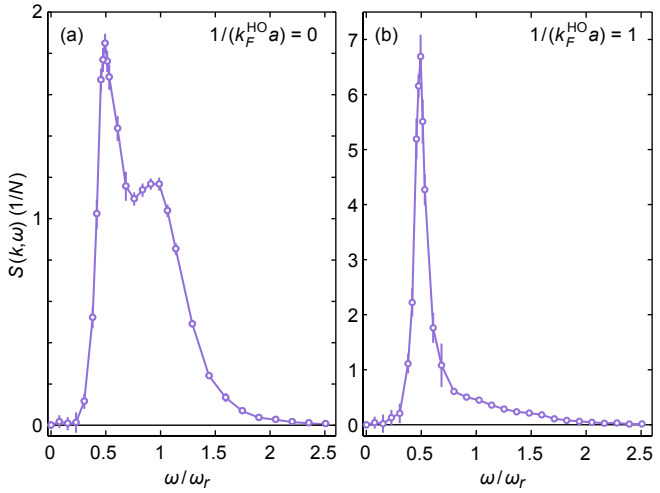

FIG. 1. (color online) Density response functions of a strongly interacting Fermi gas (a) in the unitary limit (833 G) and (b) for $k_F^{\rm HO}a = 1$ (783 G), as a function of ω/ω_r. These are equivalent to the dynamic structure factor $S(k,\omega)$ at the high momentum used for the measurement ($k = 4.46k_F^{\rm HO}$).

being sensitive to fluctuations in the initial cloud position. We also perform a careful check of the response of the cloud at various Bragg frequencies in order to determine the maximum Bragg intensity we can use and remain in the linear response regime [19]. We can therefore maximize the signal-to-noise ratio at any given Bragg frequency by using the highest beam intensity that is within the linear region. Scaling the data by the product of the Bragg beam intensities thereby allows us to combine data measured at different intensities into a single spectrum. With these techniques, and by averaging approximately ten measurements at each ω, we dramatically improve our measurements of the dynamic response.

Figure 1 shows Bragg spectra obtained (a) at unitarity and (b) at $k_F^{\rm HO}a = 1$ where $k_F^{\rm HO} \equiv [2m\hbar\bar{\omega}(3N)^{1/3}]^{1/2}$ is the Fermi wavevector in a harmonic trap, m is the ^{6}Li atomic mass and $\bar{\omega} = (\omega_x\omega_y\omega_z)^{1/3}$. These spectra contain a narrow peak at $\omega_r/2$ arising from the scattering of pairs and a broader single atom peak centred around ω_r [19]. Error bars are the statistical standard deviation of the data obtained at a particular frequency. Each spectrum is scaled by its first energy-weighted moment providing a normalized measure of the density response. At the high momentum used here ($k = 4.46k_F^{\rm HO}$) the normalized response is equivalent to the dynamic structure factor $S(k,\omega)$ [18, 20]. The normalization exploits the f-sum rule for $S(k,\omega)$, which means the quantity plotted

$$\frac{\Delta X(\omega)}{\int \omega \Delta X(\omega) d\omega} \equiv S(k,\omega)/\omega_r \qquad (1)$$

is the dynamic structure factor in units of ω_r/N where $\omega_r = \hbar k^2/(2m)$ is the recoil frequency. The integral of this normalized spectrum over ω provides the static structure factor [21] which we find to be $S(k = 4.46k_F^{\rm HO}) = 1.182 \pm 0.004$ at unitarity, and 1.48 ± 0.01 at $k_F^{\rm HO}a = 1$. This represents a dramatic improvement over previous determinations which had an error bar on the order of 10% [21].

With this precise determination of $S(k)$ we can also obtain a new measure of Tan's universal contact parameter $\mathcal{I}$ for a trapped gas at unitarity. At this high momentum, $S(k) \equiv 1 + S_{\uparrow\downarrow}(k)$ [19, 20], such that the dimensionless contact can be found directly as [22]

$$\frac{\mathcal{I}}{Nk_F^{\rm HO}} = \frac{4k}{k_F^{\rm HO}} \left(\frac{S(k) - 1}{1 - 4/(\pi k a)} \right) \qquad (2)$$

Using this expression we find $\mathcal{I}/(Nk_F^{\rm HO}) = 3.24 \pm 0.06$ at unitarity and 12.5 ± 0.2 at $k_F^{\rm HO}a = 1$. This is far more accurate than previously published data [16, 22] and sets a new benchmark for theoretical calculations of this quantity. This value is consistent with the one obtained from measurements of the equation of state [23] and from the frequency of collective oscillations [24]; however, it is significantly higher than what was found in both radio-frequency spectroscopy [25, 26] and photo-association data [27, 28]. Comparing with different theoretical results our measurements are consistent with a Nozières-Schmitt-Rink (NSR) calculation [16] and slightly below the zero temperature QMC results [29] but well above earlier many-body t-matrix calculations [30, 31]. On the BEC side our measured contact 12.5 ± 0.2 is slightly below the theoretical predictions ~ 13.2 possibly due to higher cloud temperature.

Quantum Monte Carlo calculations. We compute the ground-state properties of strongly interacting fermions in the thermodynamic limit by means of QMC techniques. We calculate for a system of 66 fermions, which has been shown to be large enough to correctly describe the thermodynamic limit [32, 33]. The QMC method has also proven to be sufficiently accurate in computing the energy as well other properties related to the contact in the unitary limit [29]. In this work, we use the same technique to calculate the dimensionless energy per particle $\xi = E/E_{FG}$ (also known as the Bertsch parameter) as a function of $(k_F a)^{-1}$, where E_{FG} is the corresponding energy for the non-interacting gas, $k_F = (3\pi^2 n)^{1/3}$ and n is the density. For each value of $(k_F a)^{-1}$ we first perform a variational optimization of the many-body wave function, which we choose to be of the same form as in Ref. [29, 34]. The best variational ansatz is then used as trial wave function in the projection in imaginary time. The fixed-node approximation is used to control the sign problem, and the accuracy of the energy and other properties depends on the quality of the variational wave function. The fixed-node energy at unitarity is within a few percent with respect to the exact calculation of Ref. [33].

For each coupling strength we perform a different QMC calculation, varying the effective range r_e of the two-body

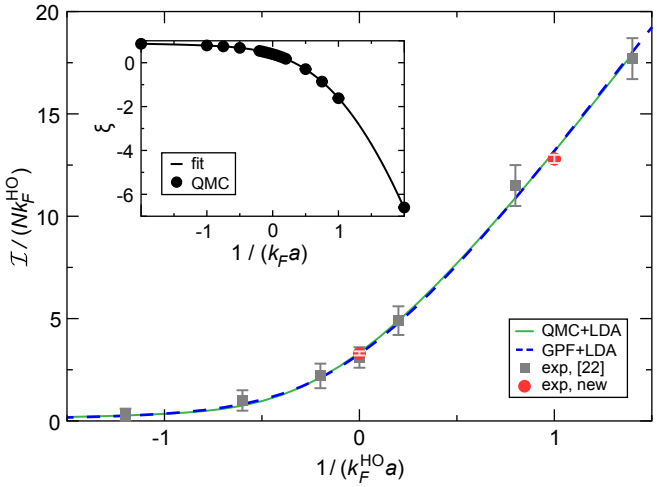

FIG. 2. (color online) The trap-averaged contact parameter as a function of $k_F^{\rm HO}a$. Green solid line is obtained from QMC data combined with the LDA and the black dotted line is a Nozières-Schmitt-Rink (NSR) calculation [16]. Red circles are the new experimental values and the grey squares are the experimental data from Ref. [22]. The inset shows the equation of state: points are the QMC simulations and the solid line is a functional fit to these. At unitarity, the experimental result is $\mathcal{I}/Nk_F^{\rm HO} = 3.24 \pm 0.06$, to be compared with the LDA value (QMC-based): 3.336 and the NSR result: 3.26 [16]. At $k_F^{\rm HO}a = 1$ the experiment yields 12.5 ± 0.2, while the LDA result is 13.17, and the NSR value is 13.20 [16].

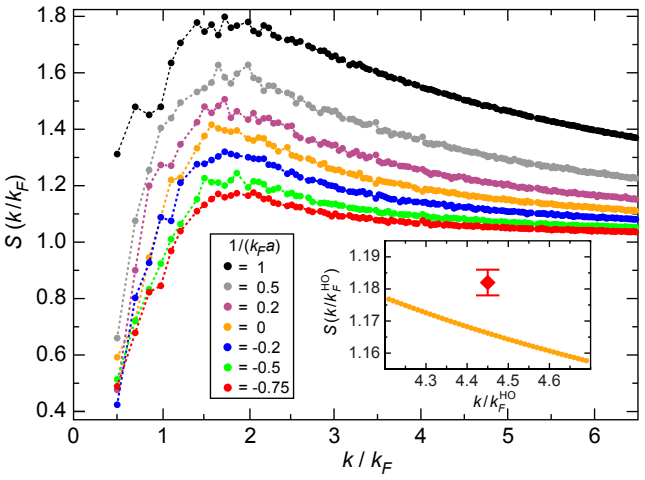

FIG. 3. (color online) Homogeneous static structure factor $S(k)$ as a function of k/k_F, for various coupling strengths computed using QMC. In the inset we compare the trap-averaged calculation of $S(k)$ at unitarity with the present experimental result (red diamond). The measurement is just over 1% higher than the QMC calculation.

interaction to extrapolate to the $r_e \to 0$ limit. This is necessary because the energy per particle ξ can be strongly dependent on r_e, depending on the value of k_Fa. For $(k_Fa)^{-1} > 0.2$, we find that the slope of $E(r_e)$ is negative and drops quickly as $(k_Fa)^{-1}$ is increased. Extrapolating to the $r_e \to 0$ limit is therefore crucial in the BEC region, while it is much less important on the BCS side of the Feshbach esonance.

The extrapolated value of ξ as a function of $(k_Fa)^{-1}$ is shown in the inset of Fig. 2. One may then use this equation of state to calculate the contact for the homogeneous system:

$$\frac{C}{Nk_F} = -\frac{6\pi}{5}\frac{\partial\xi}{\partial(k_Fa)^{-1}}\,. \tag{3}$$

Using the above equation we find a value for the contact of 3.39 at unitarity and 12.78 for $1/k_Fa = 1$.

The static structure factor is computed via

$$S(k) = \langle\rho_k^\dagger\rho_k\rangle\,, \quad \rho_k = \sum_n \exp(i\boldsymbol{k}\cdot\boldsymbol{r}_n)\,. \tag{4}$$

The QMC results for the homogeneous $S(k)$ are shown in the main panel of Fig. 3 for $(k_Fa)^{-1} = 1, 0.5, 0.2, 0, -0.2, -0.5, -0.75$ (curves from the top to the bottom in the figure), calculated at a finite effective range $r_e\,k_F = 0.056$. We have calculated the spin-parallel component of $S(k)$, and found that $S_{\uparrow\uparrow} = S_{\downarrow\downarrow} = 0.5$ within the error bars for $k > 4k_F$ in agreement with [20] and the experimental measurement of [19].

Local density approximation. Knowing the homogeneous contact and structure factor we can compute the trap-averaged values for these quantities using the local density approximation (LDA). The overall chemical potential μ is related to the local chemical potential $\mu(r)$ by $\mu = \mu(r) + V(r)$, where $V(r)$ is the trapping potential. At unitarity,

$$\mu(r) = \xi\varepsilon_F(r) = \xi\frac{\hbar^2}{2m}\left(3\pi^2 n(r)\right)^{2/3}. \tag{5}$$

Here $\varepsilon_F(r)$ is the local Fermi energy, $n(r)$ is the density profile, and we have assumed that ξ does not depend on r (valid in the unitary and free-gas limits); more generally we have $\xi = \xi(k_F(r)a)$, where $k_F(r) = (3\pi^2 n(r))^{1/3}$ and a is the scattering length. For a harmonic trapping potential $V(r) = \frac{1}{2}m\omega^2 r^2$, the density profile is given by

$$n(r) = n(0)\left[1 - \frac{r^2}{R^2}\right]^{3/2}, \qquad R \equiv \left(\xi\varepsilon_F(0)\frac{2}{m\omega^2}\right)^{1/2}, \tag{6}$$

and $n(0)$ is determined by the total number of particles in the system through the normalization condition $\int d^3r\; n(r) = N$. Given ξ, N and the frequency of the trap ω, we completely determine the ground-state density profile. Within the LDA, the total contact in a trap is given by $\mathcal{I} = \int d^3r\; \mathcal{I}(r)$, where

$$\frac{\mathcal{I}(r)}{n(r)k_F(r)} = c_0 = \frac{C}{Nk_F}, \tag{7}$$

and C is obtained from QMC data using Eq. (3). Using the density profile above, the contact in the trap is

$$\frac{\mathcal{I}}{Nk_F^{\rm HO}} = \frac{256}{105\pi} c_0 \xi^{-1/4}. \tag{8}$$

In Fig. 2 we show the contact obtained from QMC simulation (solid green line), compared with the new experimental data presented in this letter (red circles) and the experimental data of Ref. [22] (grey squares). The LDA for the static structure factor in a trap is

$$\mathcal{S}(k/k_F^{\rm HO}) = \frac{1}{N}\int d^3r\ n(r) S(k/k_F(r)), \tag{9}$$

where the dimensionless function $S(k/k_F)$ was determined via QMC. The inset of Fig. 3 shows the trap-averaged QMC result at unitarity. Also shown is the experimental measurement which lies just over 1% above the theory. Note that the LDA is less precise for $\mathcal{S}(k/k_F^{\rm HO})$ than for the energy (and contact) as fits to the QMC data are less reliable for $S(k)$, and because $S(k)$ is computed at a small but finite effective range.

Away from unitarity $\xi = \xi(k_F a)$, and

$$\frac{\mu}{\varepsilon_F} = \xi(k_F a) + \frac{1}{6\pi k_F a}\frac{C(k_F a)}{Nk_F}, \tag{10}$$

which follows from $E = -PV + \mu N$ combined with $E = \frac{3}{2}PV - \frac{\hbar^2}{8m\pi a}C$. As in the unitary case, the central density determines μ, and the LDA equation $\mu = \mu(r) + V(r)$ determines the density profile, which is solved numerically as $k_F a$ depends on r through $k_F(r)$.

Homogeneous zero-temperature contact. While our measurements were performed on a trapped (inhomogeneous) cloud our result at unitarity also provides a strong constraint on the zero temperature homogeneous contact. At finite temperatures the equation of state for the unitary Fermi gas is not known exactly, but for $T \ll T_c$, where T_c is the superfluid transition temperature, trap averaged measurements are only weakly affected by the small population in the high temperature wings. Comparing calculations of the finite temperature trapped contact based on different models for the equation of state [16, 30, 31] one finds that the ratio $\mathcal{I}(T)/\mathcal{I}(0)$ has a very weak temperature dependence in the range $0 < T/T_F < 0.08$ with a relative discrepancy of less than 1% for the different models. Thus, with knowledge of the trapped contact at a temperature $T(\ll T_c)$, it is straightforward to obtain the zero temperature trapped contact with relatively low error.

This procedure relies on a precise determination of the temperature which we achieve by fitting the finite temperature equation of state for the pressure [35] to the measured pressure obtained from one-dimensional (doubly integrated) density profiles [36, 37]. With this method we find a temperature of $T/T_F = 0.067 \pm 0.010$. We then use the zero temperature relation Eq. (8) which connects the trapped contact to the homogeneous contact c_0 [16] and find $c_0 = 3.33 \pm 0.07$ for the zero temperature homogeneous contact density, in a very good agreement with the QMC result [29]. The increased error bar is primarily due to the uncertainty in the temperature measurement. We have used $\xi = 0.376 \pm 0.004$ [38] but note that the uncertainty in ξ barely impacts the overall uncertainty as it appears in Eq. (8) to the 1/4-th power. An additional uncertainty arises due to the error bar on the precise magnetic field of the Feshbach resonance [39]. Based on a recent determination [40], and our measurement performed at 833.0 G, our unitarity result for the contact would be shifted up by 0.07.

In summary we have presented a high precision determination of the low temperature dynamic and static structure factors and contact of a strongly interacting Fermi gas. These systems are an ideal testbed for validating different many-body calculations where exact predictions are not available. Our measurements are now at a level that can discriminate between several of the established predictions and agreement with the latest QMC calculations is at the level of 1%. The measurement at unitarity also provides a new benchmark, accurate to the 2% level, for the $T \to 0$ limit of the homogeneous contact density which complements a recent measurement [26] at higher temperatures.

Acknowledgements. We would like to thank F. Werner for providing Bold Diagrammatic Monte Carlo data for the pressure equation of state and J. Carlson for useful discussions. The work of J.E.D. and S.G. was supported by a grant from the Department of Energy (DOE) under contracts DE-FC02-07ER41457 (UNEDF SciDAC), and DE-AC52-06NA25396 (LANL). Computer time was made available by Los Alamos Open Supercomputing, and by the National Energy Research Scientific Computing Center (NERSC).

[1] S. Giorgini, L. P. Pitaevskii, and S. Stringari, Rev. Mod. Phys. **80**, 1215 (2008);
I. Bloch, J. Dalibard, and W. Zwerger, Rev. Mod. Phys. **80**, 885 (2008).
[2] D. B. Kaplan, M. J. Savage, and M. B. Wise, Phys. Lett. B **424**, 390 (1998); Nucl. Phys. B **534**, 329 (1998).
[3] A. Gezerlis and J. Carlson, Phys. Rev. C **77**, 032801 (2008).
[4] T. Schaefer, Physics **2**, 88 (2009).
[5] T. Schäfer and D. Teaney, Rept. Prog. Phys. **72**, 126001 (2009).
[6] T.-L. Ho, Phys. Rev. Lett. **92**, 090402 (2004).
[7] H. Heiselberg, Phys. Rev. A **63**, 043606 (2001).
[8] E. Braaten and H.-W. Hammer, Phys. Rept. **428**, 259 (2006).
[9] W. Zwerger, *The BCS-BEC crossover and the Unitary Fermi Gas* (Springer, Berlin, 2011).
[10] S. Tan, Ann. Phys. **323**, 2952 (2008); Ann. Phys. **323**,

2971 (2008); Ann. Phys. **323**, 2987 (2008).
[11] E. Braaten and L. Platter, Phys. Rev. Lett. **100**, 205301 (2008).
[12] S. Zhang and A. J. Leggett, Phys. Rev. A **77**, 033614 (2008).
[13] E. Braaten, D. Kang, and L. Platter, Phys. Rev. Lett. **104**, 223004 (2010).
[14] D. T. Son and E. G. Thompson, Phys. Rev. A **81**, 063634 (2010).
[15] E. Taylor and M. Randeria, Phys. Rev. A **81**, 053610 (2010).
[16] H. Hu, X.-J. Liu, and P. D. Drummond, New J. Phys. **13**, 035007 (2011).
[17] Y. Nishida, Phys. Rev. A **85**, 053643 (2012).
[18] G. Veeravalli, E. Kuhnle, P. Dyke, and C. J. Vale, Phys. Rev. Lett. **101**, 250403 (2008).
[19] S. Hoinka, M. Lingham, M. Delehaye, and C. J. Vale, Phys. Rev. Lett. **109**, 050403 (2012).
[20] R. Combescot, S. Giorgini, and S. Stringari, Europhys. Lett. **75**, 695 (2006).
[21] E. D. Kuhnle, H. Hu, X.-J. Liu, P. Dyke, M. Mark, P. D. Drummond, P. Hannaford, and C. J. Vale, Phys. Rev. Lett. **105**, 070402 (2010).
[22] E. D. Kuhnle, S. Hoinka, H. Hu, P. Dyke, P. Hannaford, and C. J. Vale, New J. Phys. **13**, 055010 (2011).
[23] N. Navon, S. Nascimbène, F. Chevy, and C. Salomon, Science **328**, 729 (2010).
[24] Y. Li and S. Stringari, Phys. Rev. A **84**, 023628 (2011).
[25] J. T. Stewart, J. P. Gaebler, T. E. Drake, and D. S. Jin, Phys. Rev. Lett. **104**, 235301 (2010).
[26] Y. Sagi, T. E. Drake, R. Paudel, and D. S. Jin, arXiv:1208.2067 [cond-mat.quant-gas] (2012).
[27] G. B. Partridge, K. E. Strecker, R. I. Kamar, M. W. Jack, and R. G. Hulet, Phys. Rev. Lett. **95**, 020404 (2005).
[28] F. Werner, L. Tarruell, and Y. Castin, Eur. Phys. J. B **68**, 401 (2009).
[29] S. Gandolfi, K. E. Schmidt, and J. Carlson, Phys. Rev. A **83**, 041601 (2011).
[30] F. Palestini, A. Perali, P. Pieri, and G. C. Strinati, Phys. Rev. A **82**, 021605 (2010).
[31] T. Enss, R. Haussmann, and W. Zwerger, Ann. Phys. **326**, 770 (2011).
[32] M. M. Forbes, S. Gandolfi, and A. Gezerlis, Phys. Rev. Lett. **106**, 235303 (2011).
[33] J. Carlson, S. Gandolfi, K. E. Schmidt, and S. Zhang, Phys. Rev. A **84**, 061602(R) (2011).
[34] J. Carlson, S.-Y. Chang, V. R. Pandharipande, and K. E. Schmidt, Phys. Rev. Lett. **91**, 050401 (2003).
[35] K. Van Houcke, F. Werner, E. Kozik, N. Prokof'ev, B. Svistunov, M. J. H. Ku, A. T. Sommer, L. W. Cheuk, A. Schirotzek, and M. W. Zwierlein, Nat. Phys. **8**, 366 (2012).
[36] S. Nascimbene, N. Navon, K. J. Jiang, F. Chevy, and C. Salomon, Nature **463**, 1057 (2010).
[37] T.-L. Ho and Q. Zhou, Nat. Phys. **6**, 131 (2010).
[38] M. J. H. Ku, A. T. Sommer, L. W. Cheuk, and M. W. Zwierlein, Science **335**, 563 (2012).
[39] M. Bartenstein, A. Altmeyer, S. Riedl, R. Geursen, S. Jochim, C. Chin, J. H. Denschlag, R. Grimm, A. Simoni, E. Tiesinga, C. J. Williams, and P. S. Julienne Phys. Rev. Lett. **94**, 103201 (2005).
[40] S. Jochim, private communication (2012).